ACS Sustainable Resource Management

pubs.acs.org/acssrm

Article

From Waste to Aerogel: Upcycling of Post-Consumer Aluminum Beer Cans into Alumina-Based Aerogels with Improved Electrochemical Storage Performance

Joseane Caroline Bernardes, Hemily da Costa Guedes, Thales Mascarelli, Vinicius Augusto da Silva, Leonardo Marchiori, Klaiani Bez Fontana, Eduardo Sidinei Chaves, Carlos Renato Rambo, Sidney José Lima Ribeiro, and Elias Paiva Ferreira-Neto*

Cite This: *ACS Sustainable Resour. Manage.* 2025, 2, 1906–1916

Read Online

ACCESS | Metrics & More | Article Recommendations | Supporting Information

ABSTRACT: In this study, we report a facile, template-free, and sustainable upcycling route for the synthesis of alumina-based aerogels from post-consumer aluminum beer can waste. The developed route employs different parts of aluminum beer cans to yield phase-pure γ-AlOOH and γ-Al_2O_3 aerogels with high surface area, mesoporosity, a fine microstructure of interconnected nanoflakes/nanofibers, and good thermal stability, displaying properties that are comparable, or even superior to, those of control samples prepared from high-purity $AlCl_3$. Notably, we demonstrate that incorporation of impurities from the can alloy composition, particularly Mn, influences the optical, structural, and electrochemical behavior of prepared alumina-based aerogels, leading to a significantly improved energy storage performance in comparison to aerogels prepared with high-purity precursors. These findings establish a circular-economy-based approach to upcycle aluminum packaging waste into advanced, nanostructured aerogel materials with promising applications in energy storage, catalysis, thermal insulation, adsorption, sensing, and optical devices.

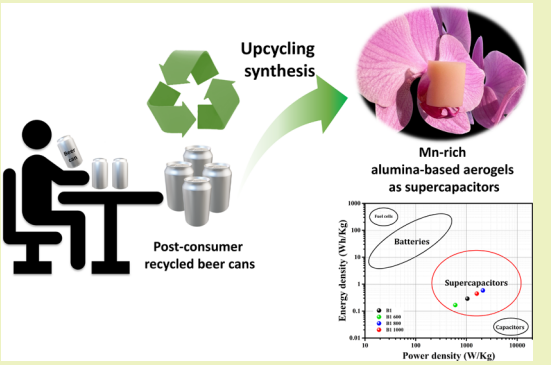

KEYWORDS: *aerogels, supercapacitor, waste valorization, upcycling, aluminum*

1. INTRODUCTION

Aerogels are a unique class of nanoporous materials created through the controlled drying of gels by replacing the solvent entrapped in gel pores with air, employing special drying conditions (e.g., supercritical drying and freeze-drying, among others) to prevent shrinkage and pore structure collapse. The as-obtained 3D monolithic structures are characterized by high surface area, high pore volume, interconnected pore structure, and low density.[1] Metal oxide aerogels, in particular, exhibit a unique set of textural, optical, structural, and surface properties, enabling exceptional performance in applications such as catalysis, water treatment, photonic technologies, energy applications, and thermal insulation.[2−4] However, traditional metal oxide gel synthesis routes often rely on expensive, toxic, and humidity-sensitive precursors,[5] which may increase costs and hinder large-scale production. In this context, the development of alternative synthesis routes that utilize raw materials or even recycled waste for the preparation of high-quality functional aerogel materials for various applications is of great interest.[6]

Solid waste management is one of the greatest environmental challenges facing modern society. While recycling processes for some materials are well developed worldwide, increased global consumption and rising waste generation create an urgent necessity for innovative and sustainable solutions for material reutilization and a circular economy. Aluminum is the most utilized non-ferrous metal in the world, with worldwide annual production exceeding 72 million tons in 2024, according to International Aluminum Institute (IAI) data.[7] Primary production of aluminum involves bauxite mining and metal smelting, processes that are energy-intensive and major greenhouse gas emitters. In fact, estimates indicate that primary aluminum production emits seven to nine times more CO_2 per ton of metal produced than steel.[7,8] On the other hand, secondary production by aluminum recycling can save up to 93% in energy in comparison to primary production. Thus, reutilization of post-consumer aluminum scrap has a key role in achieving sustainable aluminum circular economy. In particular, post-consumer aluminum beverage cans constitute

Received: May 25, 2025
Revised: October 2, 2025
Accepted: October 3, 2025
Published: October 8, 2025

an important type of aluminum waste considering their widespread usage in food industry, constituting up to 90% of beverage cans produced worldwide.[9] While recycling of post-consumer aluminum cans is a well-established process, there is still room for improvement with respect to both regulations and technological advances. Estimates indicate that roughly 70% of such waste is recycled worldwide,[9] and the presence of alloying elements in the different Al-based alloys employed to manufacture beverage cans can be problematic for complete recycling, as it is often necessary to supplement primary-produced aluminum to adjust impurity concentrations.[10,11]

In this context, upcycling emerges as an attractive approach to prepare functional advanced materials by reutilizing plastic, metal, or inorganic mineral waste.[12,13] Although several studies have reported the use of aluminum waste to prepare functional materials,[14−20] few have explored the preparation of aerogels from recycled aluminum. For instance, in 2023, the Duong group reported the preparation of Al metal/carboxymethyl/polyacrylic acid composite aerogels by grinding commercial aluminum foil into a fine powder, dispersing it into the polymer binders to form a hydrogel, and processing it by freeze-drying, characterizing it more precisely as a "cryogel".[21] The same group employed a similar freeze-drying approach for the design of $Al(OH)_3$/PVA composite aerogels.[22] While these methods produce materials with excellent performance for thermal insulation and oil absorption, the proposed approaches are dependent on the addition of polymer binders and templates and are limited to commercial aluminum foils. The present study proposes effective utilization of post-consumer aluminum cans to design alumina-based aerogels without polymer binders, particularly focusing on the previous unexplored role of impurities on the properties of the prepared functional materials. We report a facile template-free upcycling approach to prepare γ-AlOOH (boehmite) and γ-Al_2O_3 nanocrystalline aerogels from post-consumer aluminum beer cans and show their application as electrochemical capacitors. Importantly, we demonstrate that aerogel materials derived from upcycled beer cans exhibit improved electrochemical storage performance compared with aerogels produced via the conventional route with high-purity precursors. This enhancement is mainly attributed to the advantageous presence of the Mn alloying element in the aluminum alloy employed in beer cans. Moreover, the developed alumina-based aerogels by the upcycling route show high surface area, high pore volume, fine microstructure of interconnected nanoflakes/nanofibers, crystalline phase purity, and good thermal stability, making them interesting candidates for various other applications, including catalysis, adsorption, sensors, and optical devices.

2. EXPERIMENTAL SECTION

2.1. Aerogels Synthesis. Post-consumer aluminum beer cans from various local brands were collected, washed, and sanded to remove the paint layer. After the cans were sanded to completely remove the outer paint layer, each part was cut into small pieces to facilitate dissolution. The different can parts (1.08 g) were dissolved in 20 mL of concentrated HCl (37%, Exodus) under stirring at room temperature for 24 h, followed by simple filtration to obtain clear, bright yellow aqueous metal chloride precursor solutions. To prepare the Al_2O_3-based gels, a facile epoxide-assisted gelation method was employed. Briefly, 2 mL of the precursor solution was mixed with 8 mL of absolute ethanol (99%, Synth) in a centrifuge tube and homogenized by shaking. To promote gelation, 4 mL of propylene oxide (97%, Sigma-Aldrich) were added. After further homogenization, the resulting solution was quickly poured into molds and left undisturbed to gel within a few minutes. Control samples were also synthesized using a conventional sol−gel method with high-purity $AlCl_3$ (99% Sigma-Aldrich) as the aluminum source. For this synthesis, the gels were prepared following the same route described above, with the only modification being the use of 0.53 g of $AlCl_3$ instead of the precursor solution derived from recycled cans.

After gelation, two different solvent exchange and drying procedures were employed to obtain alumina-based aerogels, designated as procedure A and procedure B. Procedure A began with aging and solvent exchange of the gels in an absolute ethanol bath for 7 days, with the solvent being replaced each 24 h. The ethanol-soaked gels were then subjected to a supercritical CO_2 drying step by using an E3000 critical point dryer (Quorum Technologies). Solvent exchange with liquid CO_2 was performed for 4 h, followed by supercritical drying at 45 °C and a pressure of 1200−1300 psi for 1 h, followed by slow venting. Procedure B aging and solvent exchange of the gels was carried out in an isopropanol bath for 7 days, with the solvent being replaced each 24 h. For these isopropanol-soaked gels, the supercritical CO_2 drying process was carried out in an Autosamdri 931 critical point dryer (Tousimis). Solvent exchange with liquid CO_2 was performed for 2 h, followed by supercritical drying at 31 °C and a pressure of 1100 psi for 1 h, followed by slow venting. After drying, the aerogel samples were subjected to thermal treatments in a muffle furnace at a heating rate of 10 °C·min^{-1} under an ambient atmosphere. The samples were heated to temperatures of 600 °C, 800 °C, and 1000 °C for 2 h to investigate the formation of crystalline Al_2O_3 phases. Table 1 summarizes the different aerogel samples prepared, including their respective sample codes, the recycled aluminum can parts used to prepare the precursor solutions, thermal treatment temperature, and the drying procedures employed.

Table 1. Summary of Prepared Aerogel Samples, Detailing Sample Codes, Precursor Sources, Thermal Treatment Temperature, and Drying Procedures[a]

Sample code	Aluminum can part or precursor employed	Thermal treatment temperature	Drying procedure	Specific capacitance
A1	body	as-prepared	A	212 mF g^{-1}
A1 600	body	600 °C	A	
A1 800	body	800 °C	A	
A1 1000	body	1000 °C	A	
A2	lid	as-prepared	A	217 mF g^{-1}
A3	bottom	as-prepared	A	230 mF g^{-1}
B1	body	as-prepared	B	715 mF g^{-1}
B1 600	body	600 °C	B	413 mF g^{-1}
B1 800	body	800 °C	B	1443 mF g^{-1}
B1 1000	body	1000 °C	B	1098 mF g^{-1}
Ct	$AlCl_3$ (control sample)	as-prepared	B	611 mF g^{-1}
Ct 600	$AlCl_3$ (control sample)	600 °C	B	609 mF g^{-1}
Ct 800	$AlCl_3$ (control sample)	800 °C	B	687 mF g^{-1}
Ct 1000	$AlCl_3$ (control sample)	1000 °C	B	249 mF g^{-1}

[a]Specific capacitance values for selected samples are also shown and discussed latter on the Electrochemical Analyses section.

2.2. Structural, Chemical Composition, and Electrochemical Analysis. Experimental details for the characterization of structural, chemical composition and electrochemical properties of prepared aerogels are given the Supporting Information.[23−25]

3. RESULTS AND DISCUSSION

3.1. Synthesis, Compositional Analysis, and Impurities Presence. The reaction between Al-containing can

https://doi.org/10.1021/acssusresmgt.5c00216
ACS Sustainable Resour. Manage. 2025, 2, 1906−1916

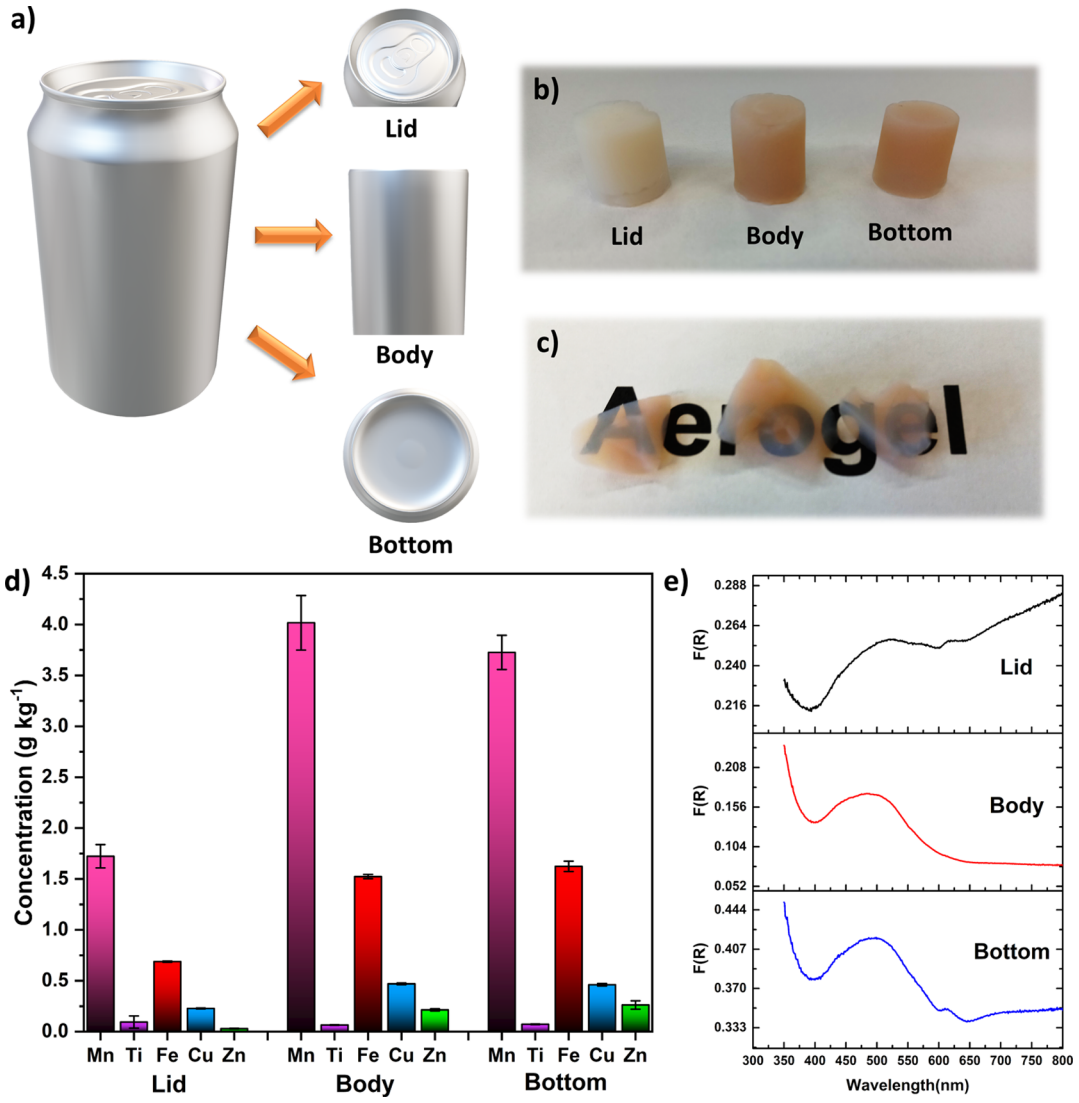

Figure 1. (a) Illustrative scheme showing different parts of aluminum beer cans used to prepare alumina-based aerogels. Photographs showing the (b) physical appearance and color of aerogel monoliths prepared using different parts of aluminum beer cans (A1−A3 samples) and (c) transparency of aerogel pieces (A1 sample). Elemental composition and optical absorption of alumina-based aerogels derived from different aluminum can parts. (d) Comparison of transition metal impurities in aerogel samples determined by ICP−MS, highlighting increased Mn and Fe content in body- and bottom-derived aerogels (Mg concentration was omitted for better comparison of transition metal impurities). (e) DRS-UV-Vis electronic absorption spectra displaying absorption bands in the visible region, associated with Mn(II) and Mn(III)-related electronic transitions.

pieces dissolved in concentrated HCl in the precursor solutions produces $AlCl_3$ and releases hydrogen gas, according to eq 1

$$2Al_{(s)} + 6HCl_{(aq)} \rightarrow 2AlCl_{3(aq)} + 3H_{2(g)} \quad (1)$$

This dissolution method offers an energy-efficient approach to metal recycling, as part of the energy invested in aluminum production can be recovered in the form of H_2, which can be integrated into the hydrogen economy,[26,27] while the resulting dissolved metal chloride species serve as precursors for material synthesis. Al_2O_3-based gels were obtained by the dissolution of precursor solutions in ethanol, followed by the addition of propylene oxide. This approach is based on the Gash method,[5] also known as the epoxide-assisted gelation method, in which propylene oxide acts as a proton scavenger, gradually increasing the pH of the medium and promoting the controlled hydrolysis and condensation of metal salt species. The ring-opening reaction of protonated epoxide intermediates with chloride ions drives the equilibrium irreversibly toward the formation of the stable 1-chloro-2-propanol molecule, ensuring continuous proton capture. The homogeneous gradual alkalinization promotes hydrolysis and subsequent condensation of aluminum aquohydroxo complexes. Condensation then proceeds via olation or oxolation mechanisms, leading to the formation of aluminum oxo-hydroxide networks and ultimately resulting in gelation[5,28,29] (mechanisms shown in Figure S1). The developed upcycling synthesis allows the preparation of aerogels via a facile and sustainable route, involving room-temperature steps and avoiding the use of high-purity precursors such as aluminum alkoxides and pure $AlCl_3$. This represents an important step towards sustainability, as the production of high-purity precursors typically involves multi-step synthesis routes and is energy-intensive. For instance, high-purity $AlCl_3$ is usually prepared by reacting metallic aluminum with chlorine gas under controlled

https://doi.org/10.1021/acssusresmgt.5c00216
ACS Sustainable Resour. Manage. 2025, 2, 1906−1916

conditions at high temperatures (670−850 °C),[30] making the process costly, energy-demanding, and environmentally challenging.

The resulting alumina-based gels were then subjected to solvent exchange and supercritical drying to yield aerogel monoliths, preserving the three-dimensional network and pore structure (Figure 1), with porosity estimated to be around 97.4% (see Supporting Information). The resulting aerogels exhibited different colors depending on the aluminum can part (Figure 1a) used to prepare the precursor solution. While conventional alumina aerogels are typically whitish, aerogels derived from the body and bottom parts of aluminum cans displayed a distinct reddish color (Figure 1b) and partial transparency (Figure 1c). This variation is likely due to differences in alloy composition, as aluminum can parts are manufactured using different Al−Mg−Mn alloys[11] designed to enhance mechanical properties and corrosion resistance. Consequently, these alloying elements were extracted from recycled cans and incorporated as impurities into the alumina-based matrix during the sol−gel synthesis. To investigate the presence of these impurities, we conducted chemical composition analysis of the prepared aerogels using XRF (Table 2) and ICP−MS (Table S1 and Figure 1d). Table 2 presents the bulk semiquantitative chemical composition determined by XRF for alumina-based aerogels prepared from different can parts and processed using solvent exchange/drying process A (A1−A3), along with a reference sample prepared from the body part and processed using solvent exchange/drying process B (B1). XRF analysis revealed the presence of several impurities, predominantly Mg, Mn, Fe, Cl, Ca, and Ti. The proportion of these impurities, along with the final Al_2O_3 content, was influenced by both the can part used and the drying process. Aerogels prepared from the body (A1) and bottom (A3) parts exhibited higher Mn and Fe contents, with the Al_2O_3 content reaching up to 93%. In contrast, the sample prepared from the lid (A2) contained higher Mg levels and exhibited the lowest concentration of Al_2O_3 (86%). Cl is most likely present due to the HCl treatment and remains adsorbed on the surface as Cl^- ions since no residual metal chloride phases were detected by XRD (shown later).

Table 2. Bulk Oxide Composition (Weight Fraction, %) Determined by XRF Semi-Quantitative Analysis for Alumina-Based Aerogel Samples Prepared Using Different Parts of Aluminum Beer Cans

oxide	A1 (body) (%)	A2 (lid) (%)	A3 (bottom) (%)	B1 (body) (%)
Al_2O_3	91.8	86.1	93.0	98.2
MnO	0.4	0.2	0.4	0.6
Fe_2O_3	0.3	0.1	0.3	0.3
CaO	1.2	1.3	0.8	0.2
MgO	1.8	4.0	1.3	
Cl	3.4	6.6	3.1	
P_2O_5		0.2	0.1	0.3
SiO_2	0.2	0.3	0.2	0.2
TiO_2	0.9	0.9	0.6	0.2
ZnO	0.1			<0.1
CuO	0.1		0.1	0.1
K_2O		0.1		

For a more accurate quantification of impurities, the samples were digested, and their elemental composition was determined using ICP−MS (Table S1 and Figure 1d). The ICP−MS data confirmed Mg, Mn, Ti, Fe, Zn, and Cu as the major metal impurities in the Al_2O_3-based aerogels, revealing that the sample prepared from the lid contained three times more Mg (up to 18.5 g/kg or 1.85%) than the other samples. Conversely, transition metal impurities such as Mn and Fe were more abundant in aerogels prepared from the body and bottom parts (A1 and A3), which likely contributes to their reddish coloration. This is further supported by diffuse reflectance UV−vis spectroscopy (DRS-UV-vis) data (Figure 1e), which reveal an electronic absorption band in the 400−600 nm region, particularly well-defined for these samples. These absorption features can be attributed to d−d electronic transitions of Mn dopants incorporated into the alumina lattice, resembling absorption features observed for Mn^{3+}-doped Al_2O_3.[31,32] The observed differences in aerogel composition are directly related to the distinct aluminum alloys used in beer can manufacturing. While the body and bottom parts are typically made from Mn-rich AA3004 alloy (containing up to 1.3% Mg, 1.5% Mn, 0.7% Fe, 0.3% Si, 0.25% Cu, 0.25% Zn, and 0.15% other elements[10]), the lid is generally made from Mg-rich AA5182 alloy (containing up to 5.0% Mg, 0.5% Mn, 0.35% Fe, 0.2% Si, 0.15% Cu, 0.25% Zn, 0.10% Ti, 0.10% Cr, and 0.15% other elements[10]). Finally, it is important to note that the solvent exchange-drying process also influenced the overall purity and composition of the aerogels. Compared to sample A1, sample B1 exhibited the highest Al_2O_3 content of 98.2%, increased Mn, and reduced Ca, Mg, and Cl content. These results suggest that solvent exchange using isopropyl alcohol in procedure B was more effective for the removal of Ca^{2+} and Cl^- impurities (probably adsorbed on the gel surface) before supercritical drying, whereas the ethanol solvent exchange used in procedure A retained more residual contaminants. Moreover, to the best of our knowledge, this is the first study to investigate the influence of each can part on the properties of alumina-derived materials, highlighting the important effects of chemical composition. Nevertheless, while such a systematic evaluation was necessary at the laboratory scale, separating can parts in large-scale industrial processes can be time- and energy-consuming, underscoring the importance of future studies evaluating materials prepared from fully processed unsorted aluminum cans.

3.2. Structural Analysis (FTIR, XRD, and TEM). FTIR (Figure 2a) and powder XRD (Figure 2b) analyses were conducted to characterize the chemical bonding and crystalline structure of the prepared alumina-based aerogels as well as their evolution with thermal treatments. For the as-prepared aerogel, four distinct vibrational absorption bands are present in the 400−1000 cm^{-1} region (marked with * in Figure 2a), which can be assigned to different vibrational modes of Al−O and Al−O−Al bonds in AlO_6 octahedral units within the boehmite (γ-AlOOH) structure.[33,34] Upon thermal treatment, these absorption bands become broader, which may be related to the conversion of boehmite into crystalline Al_2O_3 via dehydroxylation.[33,34] This inference is further corroborated by the evolution of the infrared absorption band at 1072 cm^{-1}, assigned to the δOH deformation vibrational mode in Al−OH sites of boehmite.[35] This band diminishes in intensity with increasing thermal treatment temperature and is absent in the sample treated at 1000 °C. A corresponding decrease in intensity is also observed for the broad absorption band centered at 3447 cm^{-1}, which corresponds to νOH stretching.[35] Finally, the absence of additional absorption

https://doi.org/10.1021/acssusresmgt.5c00216
ACS Sustainable Resour. Manage. 2025, 2, 1906−1916

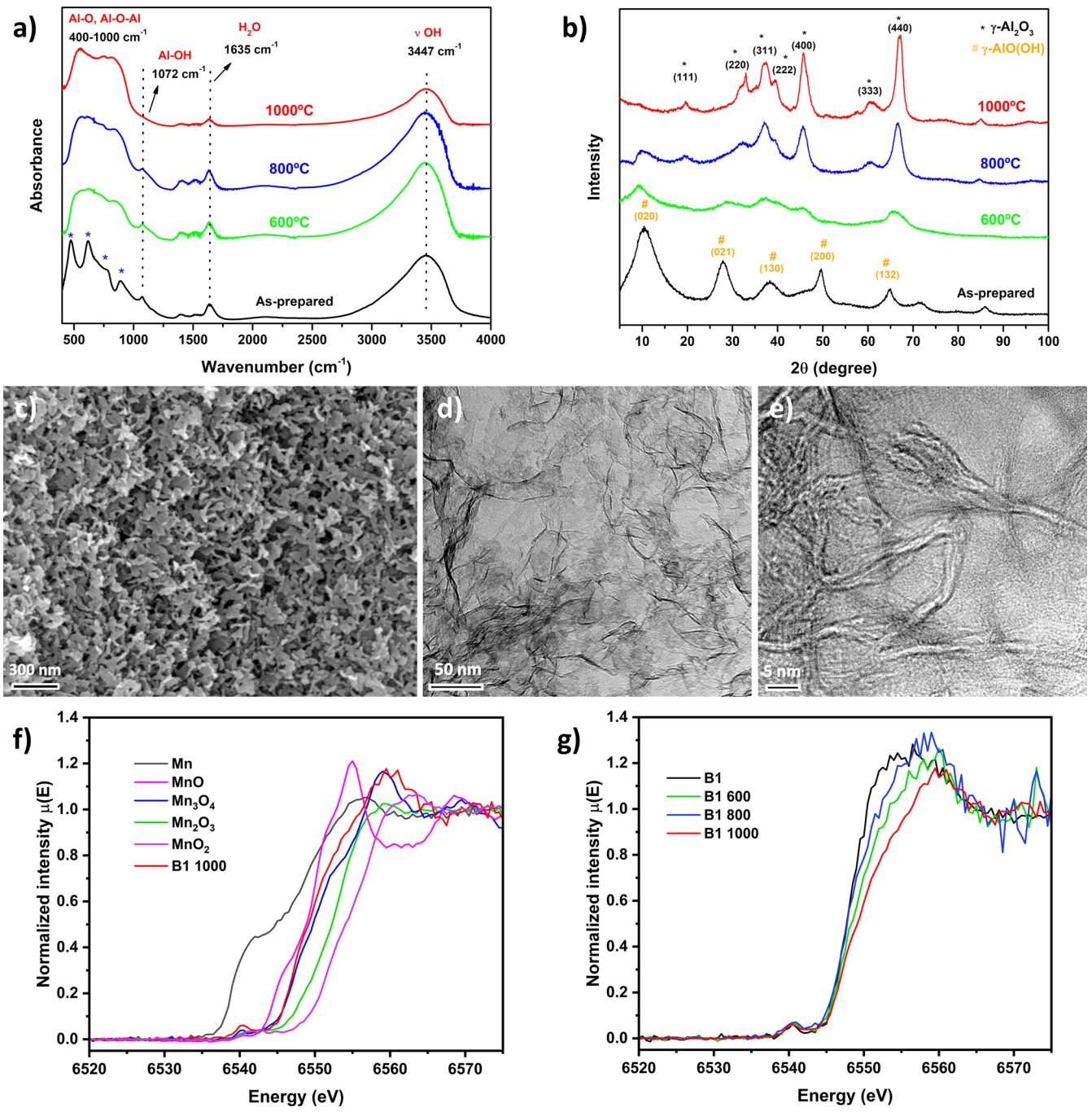

Figure 2. Structural characterization and phase transformation of alumina-based aerogels prepared from recycled beer cans: (a) FTIR spectra and (b) XRD patterns of alumina-based aerogels (sample batch A1) as-prepared and thermally treated at 600 °C, 800 °C, and 1000 °C, confirming the phase evolution from boehmite (γ-AlOOH) to γ-Al_2O_3. (c) SEM, (d) TEM, and (e) HRTEM micrographs of the γ-Al_2O_3 aerogel (A1 batch, treated at 600 °C). Mn K-edge XANES data: (f) comparison of Mn K-edge XANES spectra of manganese compounds standards to the representative spectrum of the γ-Al_2O_3 aerogel (sample B1 treated at 1000 °C). (g) Mn K-edge XANES spectra of alumina-based aerogels (B1 batch) treated at different temperatures.

bands, aside from the adsorbed water bending vibration at 1635 cm^{-1}, indicates the high purity of alumina-based aerogels from recycled cans, confirming that the process effectively removes organic contaminants and yields template-free materials.

XRD data (Figure 2b) confirm that the as-prepared aerogels crystallize in the boehmite (γ-AlOOH) phase, as indicated by the indexed diffraction pattern (ICSD #27865).[36] Consistent with FTIR analysis, the evolution of XRD diffractograms reveals the phase transformation of boehmite into γ-Al_2O_3 (ICSD #603780)[37] upon heat treatment above 600 °C, with the transition becoming complete at 1000 °C. Boehmite (γ-AlOOH) has a layered structure composed of Al−O−H sheets, where aluminum cations are coordinated in AlO_6 octahedra interconnected through edge-sharing, forming layers that are held together by hydrogen bonding between hydroxyl groups. Upon thermal treatment, the dehydroxylation process induces the phase transformation of boehmite into γ-Al_2O_3 through the

https://doi.org/10.1021/acssusresmgt.5c00216
ACS Sustainable Resour. Manage. 2025, 2, 1906−1916

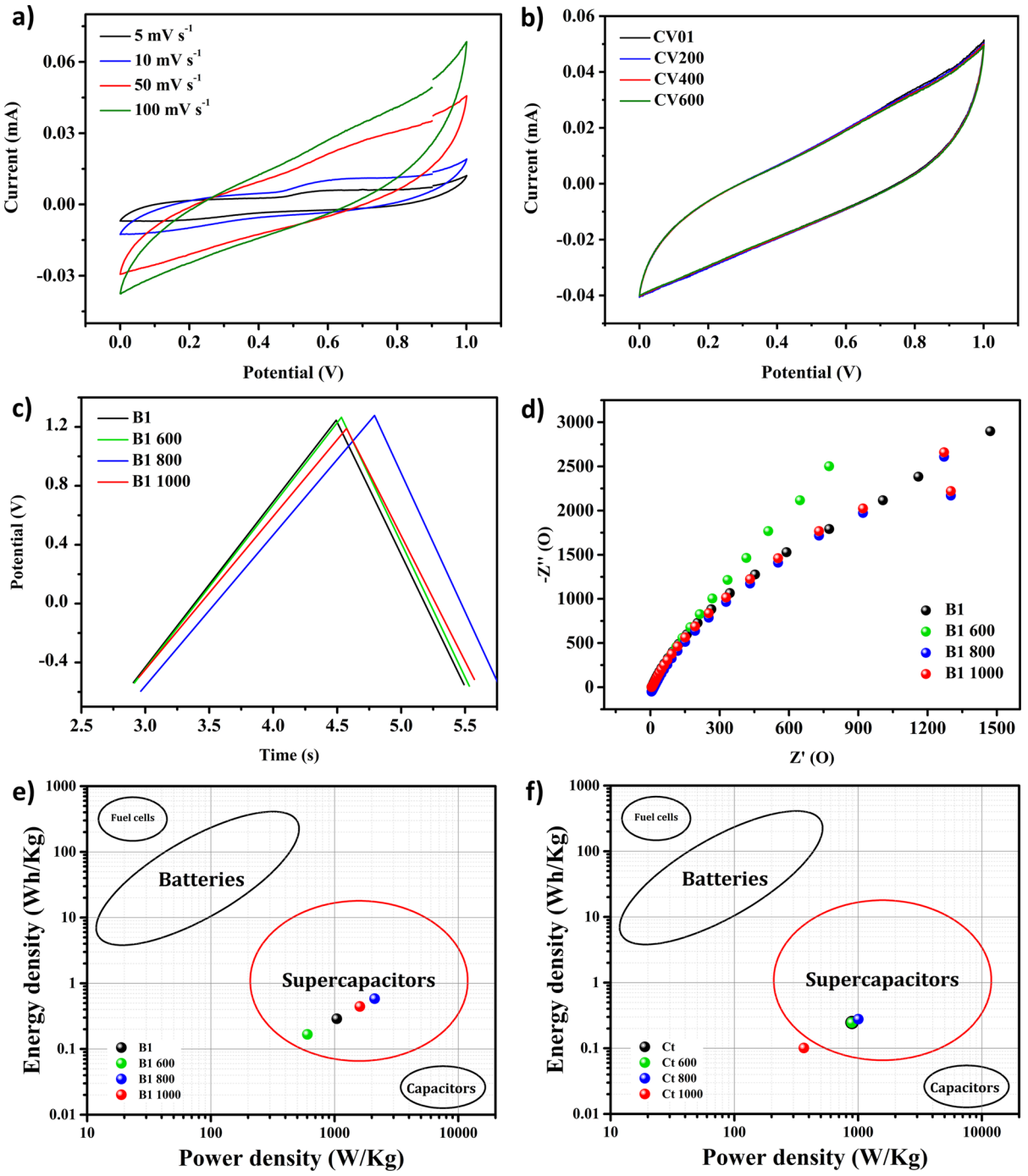

Figure 3. Electrochemical analysis of alumina-based aerogels prepared from recycled beer cans: (a) cyclic voltammetry at scan rates of 5, 10, 50, and 100 mV/s for representative alumina-based aerogel sample prepared from recycled beer cans (B1 treated at 800 °C); (b) stability of 600 cycles assessed via cyclic voltammetry at a scan rate of 100 mV/s for representative alumina-based aerogel sample prepared from recycled beer cans (B1 treated at 800 °C); (c) charge and discharge curves for alumina-based aerogels from recycled beer cans (B1 batch); (d) Nyquist plots alumina-based aerogels from recycled beer cans (B1 batch) treated at 600 °C, 800 °C, and 1000 °C; and Ragone plots for (e) alumina-based aerogels from recycled beer cans (B1 batch) and (f) control aerogels prepared with pure $AlCl_3$ treated at 600 °C, 800 °C, and 1000 °C.

gradual partial occupation of vacancies by the diffusion of Al^{3+} and O^{2-} ions (reaction mechanism), as proposed by Luo based on electron diffraction data.[38] While the exact structure of γ-Al_2O_3 remains under discussion,[39] it is most commonly described as a defective cubic spinel structure with space group $Fd\bar{3}m$,[37] where aluminum cations occupy both tetrahedral and octahedral sites and intrinsic cation vacancies are required to satisfy the 2:3 stoichiometry.[40] Additionally, a tetragonal distortion of the cubic structure into $I4_1/amd$ is frequently proposed based on neutron diffraction, transmission electron microscopy,[41] and XRD data.[42] It is important to note that the XRD data of alumina-based aerogels prepared from cans indicate the presence of only boehmite or alumina, with no detectable secondary crystalline phases associated with the inorganic contaminants identified by XRF and ICP−MS analyses. This observation may be attributed to the low

https://doi.org/10.1021/acssusresmgt.5c00216
ACS Sustainable Resour. Manage. 2025, 2, 1906−1916

concentrations of such potential phases, falling below the XRD detection limit, or to the incorporation of impurities as dopants within the γ-AlOOH or γ-Al_2O_3 crystalline lattices.

Figure 2c shows a representative SEM micrograph of the prepared γ-Al_2O_3 aerogel, depicting the surface texture of an open-porous structure with a flake-like morphology. B1 batch aerogels (Figure S2) exhibited a slightly more compact structure compared to the A1 batch sample (Figure 2c), indicating the influence of the drying procedure on the microstructure. The open-porous architecture was largely retained after thermal treatment up to 800 °C; however, a significant reduction in porosity was observed after treatment at 1000 °C (Figure S2). Figure 2d,e displays TEM and HRTEM micrographs at different magnifications for γ-Al_2O_3 aerogels (treated at 600 °C). TEM micrographs reveal that aerogel consists of a 3D network of interconnected nanoflakes of variable lengths. HRTEM images reveal that these nanoflakes exhibit a fibrous structure with a diameter of less than 5 nm. Such a unique microstructure was previously observed in Al_2O_3 aerogels synthesized using a pure $AlCl_3$ precursor and the epoxide-assisted gelation method, as reported by Baumann and co-authors.[28] This indicates that impurities from recycled cans do not alter the aerogel microstructure, allowing the formation of a fine nanostructure from a lower-purity aluminum source. Moreover, comparison between TEM/HRTEM micrographs of γ-AlOOH and γ-Al_2O_3 aerogels (Figure S3) reveal that the microstructure remains practically unchanged after thermal treatment, aside from the increased crystallinity of the nanoflake structure in the γ-Al_2O_3 aerogel compared to that in the γ-AlOOH aerogel. This behavior points to the high thermal stability of the prepared aerogels and reflects the topotactic phase transformation of boehmite to γ-Al_2O_3 via thermal dehydration, which commonly preserves the original morphology and microstructure of the crystallites.[38,43]

Due to its importance for electrochemical performance, the chemical state of the Mn species in the prepared alumina-based aerogels was investigated by XPS and Mn K-edge XANES. The XPS spectrum of a representative γ-Al_2O_3 aerogel sample (Figure S4) confirms the presence of Mn surface species, showing a Mn $2p_{3/2}$ peak at a binding energy of ∼642.4 eV, consistent with values reported for MnO_x species supported on γ-Al_2O_3.[44] Further insights into the oxidation state of Mn species were obtained from Mn K-edge XANES, as the absorption edge energy (E_0) is sensitive to oxidation state,[45] as shown by comparison with standard compounds (Figure 2f and Table S2). The Mn species in alumina-based aerogels exhibit E_0 = 6547.5 ± 0.5 eV, which closely matches the Mn_3O_4 standard (6547.5 eV), indicating the coexistence of Mn(II) and Mn(III). Upon thermal treatment, the main absorption peak gradually shifts toward higher energies (Figure 2g), suggesting the partial oxidation of Mn(II) into Mn(III). Finally, the relatively pronounced pre-edge feature (1s → 3d transition) suggests the occupancy of Mn in sites with distorted octahedral or tetrahedral symmetry.[44,45]

3.3. Porous Structure and Textural Properties Analysis. The porous structure and textural properties of the prepared alumina-based aerogels were investigated by using N_2 physisorption analysis. The corresponding isotherms, pore size distributions, and textural parameters, determined by the BET and BJH methods, are presented in Figures S5 and S6 and Table S3. All observed isotherms correspond to type IV in the IUPAC classification,[46] confirming the mesoporous nature of the materials. The hysteresis loops are classified as H1,[46] which are typically associated with a relatively uniform pore size distribution, consistent with an interconnected pore structure without pore blocking. BJH pore size distribution indicates that most materials exhibit a broad distribution of large mesopores centered around 50 nm, with the exception of the sample treated at 1000 °C, which shows a narrower distribution centered near 30 nm, likely due to the collapse of larger mesopores. As-prepared γ-AlOOH aerogels exhibit high specific surface area (SA) and pore volume (PV) values, ranging from SA: 250 $m^2\ g^{-1}$, PV: 0.89 $cm^3\ g^{-1}$ to SA: 470 $m^2\ g^{-1}$, PV: 4.70 $cm^3\ g^{-1}$, depending on the can part used and the drying procedure employed. A comparison of the data for the A1 and B1 batch samples reveals that procedure A results in materials with approximately 64% higher SA (411 $m^2\ g^{-1}$ versus 250 $m^2\ g^{-1}$) and 4.7 times higher PV (4.19 $cm^3\ g^{-1}$ versus 0.89 $cm^3\ g^{-1}$) compared to the sample prepared using procedure B. As discussed later, sample batch B showed improved performance for supercapacitor applications, which may be due to the enhanced Al_2O_3 purity and increased presence of Mn as dopant. However, for other potential applications that are directly influenced by specific surface area, such as catalysts,[47,48] supports,[49,50] and adsorbents,[51] samples prepared with procedure A may be more suitable. Additionally, both the B1 and control samples, synthesized using procedure B, exhibit similar SA and PV values, indicating that recycled post-consumer aluminum cans, despite being a low-purity aluminum source, can also yield high-surface-area aerogels. The isotherm shape for aerogels prepared from beer cans remains largely unchanged after thermal treatments (Figure S5), indicating that the overall mesoporous structure is thermally stable and preserved after annealing. While the initial conversion of γ-AlOOH aerogels into the γ-Al_2O_3 crystalline phase at 600 °C results in minimal changes in SA and PV values, more significant decreases are observed at 1000 °C. This is further corroborated by SEM and BJH analysis, which indicated that the porous structure is stable up to 800 °C.

3.4. Electrochemical Analysis. Representative electrochemical analysis data for alumina-based aerogels prepared from recycled beer cans are summarized in Figure 3, while additional data (including for control aerogel samples) are presented in the Supporting Information (Figures S7−S12). The cyclic voltammograms of the alumina-based aerogels prepared from recycled beer cans are shown in Figures 3a and S7. As expected, increasing the scan rate raises the current response due to ion migration limitations, leading to reduced electrode capacitance.[52] The CV curves display a nearly rectangular shape, characteristic of electrical double-layer capacitance but also show sloping profiles with broad redox features around 0.2 and 0.6 V, more prominent in the 1000 °C treated sample.[53] These deviations from ideal EDLC behavior indicate pseudocapacitive contributions, which arise from Faradaic processes, most likely associated with the presence of transition-metal impurities, particularly Mn, which exists as mixed-valence Mn^{2+}/Mn^{3+} species, as confirmed by XANES. The stability of the alumina-based aerogel electrodes was measured through cyclic voltammetry, evaluated at a scan rate of 100 mV/s (Figures 3b, S9, and S10). Notably, the current response remains stable over 600 cycles for all samples, with overlapping voltammetric curves, indicating excellent electrochemical stability, which is essential for supercapacitor performance.

https://doi.org/10.1021/acssusresmgt.5c00216
ACS Sustainable Resour. Manage. 2025, 2, 1906−1916

The specific capacitances of the alumina-based aerogel electrodes were calculated at each scan rate applied during cyclic voltammetry (Figure S11). Since diffusion limitations occur at higher scan rates, our discussion focuses on the specific capacitances measured at a scan rate of 5 mV/s, with these values for the different aerogel electrodes shown in Table 1. A comparison of the data for as-prepared γ-AlOOH (boehmite) aerogel samples reveals that samples prepared using solvent exchange/drying procedure B displayed up to 3.3 times higher specific capacitance compared to those prepared through procedure A, which showed relatively low specific capacitances regardless of the can part employed for the synthesis, even though procedure A led to significantly higher specific surface area aerogels. A possible explanation for this behavior is the lower purity of the aerogels prepared using procedure A (86−93% Al_2O_3), which XRF analysis revealed to have increased concentrations of Ca, Cl, and Mg impurities. In contrast, the B1 sample showed an Al_2O_3 content of above 98%, along with a higher Mn impurity content. Ca, Cl, and Mg impurities may alter the surface and electronic properties of the aerogels, for instance, by blocking surface-active sites or modifying local electrode/electrolyte interactions, which could negatively impact ion transport, ultimately reducing charge storage capability. On the other hand, Mn impurities could contribute to the improved specific capacitance of alumina-based aerogels, considering that MnO_x materials exhibit pseudocapacitive behavior through fast and reversible surface redox reactions.[54] MnO_x species have been shown to enhance the electrochemical performance of nanocomposite electrodes, particularly when combined with porous metal oxides or carbon-based materials.[55−58] Given the superior performance of the B1 sample compared to that of the A1−A3 samples, the following discussion will focus exclusively on B1-derived samples and the control aerogel prepared by using pure $AlCl_3$ with the same solvent exchange/drying procedure (procedure B).

When analyzing the data for alumina-based aerogels obtained by upcycling post-consumer beer cans (B1 batch), an increase in specific capacitance with higher heat treatment temperatures is observed, reaching an optimal value for the γ-Al_2O_3 aerogel treated at 800 °C. This behavior can be attributed to the formation of a material with increased crystallinity while maintaining a high active surface area and pore volume as well as preserving the interconnected mesoporous structure, which enhances ion flow from the electrolyte to the electrode. In contrast, specific capacitances remain relatively stable for the control aerogel samples, with a more pronounced decline observed for the aerogel calcined at 1000 °C due to its reduced surface area. This distinct behavior of the control aerogel samples as a function of thermal treatment temperature might be related to the trade-off between increased crystallinity and reduction in specific surface area induced by thermal treatment. In fact, the B1 sample demonstrated slightly higher resistance to thermal treatment, with its surface area decreasing from 250 $m^2\ g^{-1}$ to 149 $m^2\ g^{-1}$ after treatment at 800 °C, whereas the control aerogel sample showed a more significant reduction, from 247 $m^2\ g^{-1}$ to 115 $m^2\ g^{-1}$. Moreover, the B1 800 aerogel exhibited a 110% higher specific capacitance compared to the control aerogel sample treated under the same conditions (Ct 800), indicating that the Al_2O_3-based aerogel prepared via upcycling synthesis displays superior electrochemical performance. This remarkable result can be attributed to the presence of MnO_x impurities, derived from the aluminum beer can alloy, which enhance electrochemical charge storage by introducing pseudocapacitive properties in addition to the double-layer supercapacitor behavior, as previously discussed.

The charge and discharge capacity (Figures 3c and S12) of the alumina-based aerogel electrodes was evaluated at a current density of 0.5 A/g linear behavior, with fast charge and discharge times, as observed for all Al_2O_3-based aerogels, regardless of the heat treatment performed on the aerogels. The profile obtained from these aerogels by this technique may be an indication of a high-power delivery, at fast time rates, when applied in supercapacitors.[18] The impedance spectroscopy technique was used to obtain the Nyquist diagrams of the aerogel electrodes, which are presented in Figures 3d and S12. All the profiles seen in the diagram are similar, exhibiting an absence of semicircles at high frequency and a straight-line inclination along the $-Z''$ axis, suggesting a diffusion-limited capacitance at low frequencies, but a predominant double-layer capacitive behavior. It is also observed that the angles of inclination of the straight-line are very similar for all aerogels, resulting in the same impedance module, which can be described in an equivalent circuit consisting of an ideal capacitor and a parallel resistance.[59]

Using the calculated energy density (Wh/kg) and power density (W/kg) values for the aerogel electrodes, a Ragone plot (Figure 3e,f) was constructed to visually assess the applicability of these materials as electrodes in energy storage devices. Analyzing the Ragone plot in Figure 3e, which corresponds to alumina-based aerogels derived from recycled beer cans (B1 batch), all samples fall within the desirable region for supercapacitor applications, confirming their suitability as energy storage materials. In contrast, although most of the control Al_2O_3 aerogels synthesized from pure $AlCl_3$ fall within the supercapacitor region (Figure 3f), the Al_2O_3 aerogel calcined at 1000 °C exhibits both low power and high energy densities, making it unsuitable for supercapacitor applications. Another important observation is that aerogels derived from recycled aluminum exhibit higher energy and power densities compared with those synthesized from pure $AlCl_3$. This enhanced performance may be attributed to the presence of MnO_x impurities, which could contribute to pseudocapacitive charge storage in addition to double-layer capacitance, further supporting their potential as promising electrode materials for supercapacitors.

4. CONCLUSIONS

In this study, we demonstrate a sustainable and template-free upcycling strategy for the synthesis of phase-pure γ-AlOOH or γ-Al_2O_3 aerogels using different parts of post-consumer aluminum beer cans as precursor sources. Due to differences in alloy composition, the bottom and body parts yield Mn-rich aerogels, while the lid parts result in Mg-rich aerogels. Solvent exchange and drying of ethanol-soaked gels yield aerogels with high surface areas (up to 470 $m^2\ g^{-1}$) and high pore volumes (up to 4.7 $cm^3\ g^{-1}$), whereas isopropanol-soaked gels produce aerogels with higher purity and increased Mn content that are more suitable for supercapacitor applications. Importantly, we demonstrate that the alumina-based aerogels produced via the upcycling strategy show superior electrochemical storage performance as supercapacitor electrodes compared with control samples derived from high-purity precursors. This enhanced performance is attributed to the combined effects of high porosity and mesostructural integrity and the presence of

https://doi.org/10.1021/acssusresmgt.5c00216
ACS Sustainable Resour. Manage. 2025, 2, 1906−1916

MnO_x species derived from the aluminum can alloy composition, which imbue the materials with pseudocapacitive charge storage behavior. In summary, this study introduces a facile route to upcycle post-consumer aluminum cans into functional alumina-based aerogels, adding value to low-cost waste and replacing expensive precursors. The resulting aerogels feature a high surface area, pore volume, phase purity, and thermal stability, making them promising for catalysis, adsorption, sensing, and optical applications.

■ ASSOCIATED CONTENT

Supporting Information

The Supporting Information is available free of charge at https://pubs.acs.org/doi/10.1021/acssusresmgt.5c00216.

Experimental details, sol−gel mechanisms, ICP−MS data, and BET/BJH and electrochemical analysis data (PDF)

■ AUTHOR INFORMATION

Corresponding Author

Elias Paiva Ferreira-Neto − *Institute of Chemistry, São Paulo State University—UNESP, Araraquara 14800-060, Brazil;* orcid.org/0000-0002-9810-7564; Email: elias.p.ferreira@unesp.br

Authors

Joseane Caroline Bernardes − *Department of Electrical and Electronic Engineering, Federal University of Santa Catarina—UFSC, Florianópolis 88040-370, Brazil;* orcid.org/0009-0007-9094-8899

Hemily da Costa Guedes − *Department of Chemistry, Federal University of Santa Catarina—UFSC, Florianópolis 88040-380, Brazil*

Thales Mascarelli − *Institute of Chemistry, São Paulo State University—UNESP, Araraquara 14800-060, Brazil*

Vinicius Augusto da Silva − *Institute of Chemistry, São Paulo State University—UNESP, Araraquara 14800-060, Brazil*

Leonardo Marchiori − *Institute of Chemistry, São Paulo State University—UNESP, Araraquara 14800-060, Brazil*

Klaiani Bez Fontana − *Department of Chemistry, Federal University of Santa Catarina—UFSC, Florianópolis 88040-380, Brazil*

Eduardo Sidinei Chaves − *Department of Chemistry, Federal University of Santa Catarina—UFSC, Florianópolis 88040-380, Brazil*

Carlos Renato Rambo − *Department of Electrical and Electronic Engineering, Federal University of Santa Catarina—UFSC, Florianópolis 88040-370, Brazil;* orcid.org/0000-0001-5192-7277

Sidney José Lima Ribeiro − *Institute of Chemistry, São Paulo State University—UNESP, Araraquara 14800-060, Brazil;* orcid.org/0000-0002-8162-6747

Complete contact information is available at: https://pubs.acs.org/10.1021/acssusresmgt.5c00216

Funding

The Article Processing Charge for the publication of this research was funded by the Coordenacao de Aperfeicoamento de Pessoal de Nivel Superior (CAPES), Brazil (ROR identifier: 00x0ma614).

Notes

The authors declare no competing financial interest.

■ ACKNOWLEDGMENTS

Authors thank Brazilian funding agencies FAPESP (grant 21/08111-2), CNPq (Grants 407747/2022-2, 407414/2023-1, 405282/2022-2, 140851/2021-6), and CAPES/CAPES-PRINT (Grant #306745/2021-6 Project #88881.310728/2018-01), National Institutes of Science and Technology (INCTs), INCT-INFO (National Institute of Photonics), and INCT NanoVida (Nanomaterials for Life) for financial support. In accordance with ACS Publications policies, authors acknowledge ChatGPT 4.0 Large Language Model (OpenAI) for improving grammar and language of this manuscript. This research used facilities of the Brazilian Synchrotron Light Laboratory (LNLS), part of the Brazilian Center for Research in Energy and Materials (CNPEM), a private non-profit organization under the supervision of the Brazilian Ministry for Science, Technology, and Innovations (MCTI). The CARNAÚBA beamline staff is acknowledged for assistance during the experiments [Proposal 20250479]. The authors also thank Prof. Dr. Valmor R. Mastelaro (IFSC-USP) for assistance with XPS measurements, Dr. Verônica C. Teixeira (LNLS) for assistance with XANES measurements, and Dr. Caio C. dos Santos (IQ-UNESP) for assistance with helium pycnometry measurements.

■ REFERENCES

(1) Steiner, S. A.; Pierre, A. C. The Story of Aerogel. In *Springer Handbook of Aerogels*; Aegerter, M. A., Leventis, N., Koebel, M., Steiner, S. A., III, Eds.; Springer International Publishing: Cham, 2023; pp 1−50.

(2) Lee, K. H.; Arshad, Z.; Dahshan, A.; Alshareef, M.; Alsulami, Q. A.; Bibi, A.; Lee, E. J.; Nawaz, M.; Zubair, U.; Javid, A. Porous Aerogel Structures as Promising Materials for Photocatalysis, Thermal Insulation Textiles, and Technical Applications: A Review. *Catalysts* **2023**, *13* (9), 1286.

(3) Zhi, M.; Tang, H.; Wu, M.; Ouyang, C.; Hong, Z.; Wu, N. Synthesis and Photocatalysis of Metal Oxide Aerogels: A Review. *Energy Fuels* **2022**, *36*, 11359−11379.

(4) Woignier, T.; Karatum, O.; Plata, D. L. Environmental Applications for Aerogels. In *Springer Handbook of Aerogels*; Aegerter, M. A., Leventis, N., Koebel, M., Steiner, S. A., III, Eds.; Springer International Publishing: Cham, 2023; pp 1383−1398.

(5) Baumann, T. F.; Gash, A. E.; Satcher, J. H.; Leventis, N.; Steiner, S. A. Synthesis of Metal Oxide Aerogels via Epoxide-Assisted Gelation of Metal Salts. In *Springer Handbook of Aerogels*; Aegerter, M. A., Leventis, N., Koebel, M., Steiner, S. A., III, Eds.; Springer International Publishing: Cham, 2023; pp 419−435.

(6) Duong, H. M. Aerogel-Inspired Materials Derived from Industrial Waste. In *Springer Handbook of Aerogels*; Aegerter, M. A., Leventis, N., Koebel, M., Steiner, S. A., III, Eds.; Springer International Publishing: Cham, 2023; pp 1211−1237.

(7) International Aluminium Institute Primary Aluminium Production Statistics. International Aluminium Institute. https://international-aluminium.org/statistics/primary-aluminium-production/ (accessed Oct 2, 2025).

(8) Pan, Z.; Zhang, Z.; Che, D. Exploring Primary Aluminum Consumption: New Perspectives from Hybrid CEEMDAN-S-Curve Model. *Sustainability* **2023**, *15* (5), 4228.

(9) Geueke, B.; Groh, K.; Muncke, J. Food Packaging in the Circular Economy: Overview of Chemical Safety Aspects for Commonly Used Materials. *J. Clean. Prod.* **2018**, *193*, 491−505.

(10) Niero, M.; Olsen, S. I. Circular Economy: To Be or Not to Be in a Closed Product Loop? A Life Cycle Assessment of Aluminium Cans with Inclusion of Alloying Elements. *Resour. Conserv. Recycl.* **2016**, *114*, 18−31.

(11) Raabe, D.; Ponge, D.; Uggowitzer, P. J.; Roscher, M.; Paolantonio, M.; Liu, C.; Antrekowitsch, H.; Kozeschnik, E.;

Seidmann, D.; Gault, B.; De Geuser, F.; Deschamps, A.; Hutchinson, C.; Liu, C.; Li, Z.; Prangnell, P.; Robson, J.; Shanthraj, P.; Vakili, S.; Sinclair, C.; Bourgeois, L.; Pogatscher, S. Making Sustainable Aluminum by Recycling Scrap: The Science of "Dirty" Alloys. *Prog. Mater. Sci.* **2022**, *128*, 100947.
(12) Wyss, K. M.; Deng, B.; Tour, J. M. Upcycling and Urban Mining for Nanomaterial Synthesis. *Nano Today* **2023**, *49*, 101781.
(13) Zhang, F.; Wang, F.; Wei, X.; Yang, Y.; Xu, S.; Deng, D.; Wang, Y. Z. From Trash to Treasure: Chemical Recycling and Upcycling of Commodity Plastic Waste to Fuels, High-Valued Chemicals and Advanced Materials. *J. Energy Chem.* **2022**, *69*, 369−388.
(14) Mohamad, S. M.; Roslan, N. A.; Zainal Abidin, S. Comparison on the Physicochemical Properties of Alumina Extracted from Various Aluminum Wastes. *Mater. Today Proc.* **2022**, *57*, 1179−1183.
(15) Satish Reddy, M.; Neeraja, D. Aluminum Residue Waste for Possible Utilisation as a Material: A Review. *Sādhanā* **2018**, *43*, 124.
(16) Benkhelif, A.; Kolli, M. Synthesis of Pure Magnesium Aluminate Spinel (MgAl2O4) from Waste Aluminum Dross. *Waste Biomass Valorization* **2022**, *13* (5), 2637−2649.
(17) Feng, H.; Wang, L.; Li, G.; Jin, Q. Removal of Impurities for the Synthesis of High-Property Alumina-Spinel Ceramic from Secondary Aluminum Dross. *Ceram. Int.* **2023**, *49* (22), 34616−34626.
(18) Mostafa, M. M. M.; Alshehri, A. A.; Salama, R. S. High Performance of Supercapacitor Based on Alumina Nanoparticles Derived from Coca-Cola Cans. *J. Energy Storage* **2023**, *64*, 107168.
(19) Chotisuwan, S.; Sirirak, A.; Har-Wae, P.; Wittayakun, J. Mesoporous Alumina Prepared from Waste Aluminum Cans and Used as Catalytic Support for Toluene Oxidation. *Mater. Lett.* **2012**, *70*, 125−127.
(20) Esaifan, M.; Al-Mobydeen, A.; Al-Masri, A. N.; Altwaiq, A. M.; Al-Saqarat, B. S.; Mahmoud, W.; Hamaideh, A.; Moosa, I. S.; Hamadneh, I.; AlShamaileh, E. Synthesis of Nanostructured Alumina from Byproduct Aluminum Filings: Production and Characterization. *Inorganics* **2023**, *11* (9), 355.
(21) Goh, X. Y.; Ong, R. H.; Nguyen, P. T. T.; Bai, T.; Aw, D.; Li, T.; Nguyen, L. T.; Duong, H. M. Advanced Fabrication and Multi-Properties of Aluminum-Based Aerogels from Aluminum Waste for Thermal Insulation and Oil Absorption Applications. *Molecules* **2023**, *28* (6), 2727.
(22) Sp, T. S.; Nguyen, P. T. T.; Do, N. H. N.; Le, D. K.; Thai, Q. B.; Le, P. K.; Phan-Thien, N.; Duong, H. M. Advanced Fabrication and Multi-Properties of Aluminium Hydroxide Aerogels from Aluminium Wastes. *J. Mater. Cycles Waste Manag.* **2021**, *23* (3), 885−894.
(23) Pan, Q.; Liu, Q.; Shi, Y.; Yang, D.; Lan, Y.; Wang, T. A Facile Strategy for Freeze-Drying Preparation of Silica Aerogel from Sodium Silicate. *Ceram. Int.* **2025**, *51* (4), 5342−5350.
(24) Tolentino, H. C. N.; Geraldes, R. R.; Moreno, G. B. Z. L.; Pinto, A. C.; Bueno, C. S. N. C.; Kofukuda, L. M.; Sotero, A. P. S.; Neto, A. C. P.; Lena, F. R.; Wilendorf, W. H.; Baraldi, G. L.; Luiz, S. A. L.; Dias, C. S. B.; Perez, C. A.; Neckel, I. T.; Galante, D.; Teixeira, V. C.; Hesterberg, D. X-ray Microscopy Developments at Sirius-LNLS: First Commissioning Experiments at the Carnauba Beamline. *Proc. SPIE* **2021**, *11839*, 6.
(25) Ravel, B.; Newville, M. ATHENA, ARTEMIS, HEPHAESTUS: Data Analysis for X-ray Absorption Spectroscopy Using IFEFFIT. *J. Synchrotron Radiat.* **2005**, *12* (4), 537−541.
(26) Soberanis, M. A. E.; Vales-Pinzón, C.; Hernández-Núñez, E.; Flota-Bañuelos, M.; Medina, J.; Quintal-Palomo, R.; San-Pedro, L.; Ruiz-Gómez, M. Temperature Dependence on Hydrogen Production from Hydrolysis Reaction of Recycled Aluminum. *Clean Technol. Environ. Policy* **2023**, *25* (1), 35−49.
(27) Salimbeni, A.; Di Bianca, M.; Maria Rizzo, A.; Chiaramonti, D. Application of an Integrated Pyrolysis and Chemical Leaching Process for Pulper Waste Conversion into Coal, Hydrogen and Chemical Flocculating Agent. *Waste Manage.* **2024**, *174*, 549−557.
(28) Baumann, T. F.; Gash, A. E.; Chinn, S. C.; Sawvel, A. M.; Maxwell, R. S.; Satcher, J. H. Synthesis of High-Surface-Area Alumina Aerogels without the Use of Alkoxide Precursors. *Chem. Mater.* **2005**, *17* (2), 395−401.
(29) Juhl, S. J.; Dunn, N. J. H.; Carroll, M. K.; Anderson, A. M.; Bruno, B. A.; Madero, J. E.; Bono, M. S. Epoxide-Assisted Alumina Aerogels by Rapid Supercritical Extraction. *J. Non-Cryst. Solids* **2015**, *426*, 141−149.
(30) Helmboldt, O.; Keith Hudson, L.; Misra, C.; Wefers, K.; Heck, W.; Stark, H.; Danner, M.; Rösch, N. Aluminum Compounds, Inorganic. In *Ullmann's Encyclopedia of Industrial Chemistry*; Wiley, 2007; pp 1−17.
(31) van Die, A.; Leenaers, A. C. H. I.; van der Weg, W. F.; Blasse, G. A Search for Luminescence of the Trivalent Manganese Ion in Solid Aluminates. *Mater. Res. Bull.* **1987**, *22* (6), 781−788.
(32) Khomenko, O. V.; Berezovskaya, I. V.; Stoyanova, I. V.; Efryushina, N. P.; Dotsenko, V. P.; Poletaev, N. I.; Khlebnikova, M. E. Synthesis and Luminescence Study of Mn-Doped Nanosized Al2O3. In *2018 IEEE 8th International Conference Nanomaterials: Application & Properties (NAP)*, 2018, pp 1−4.
(33) Caiut, J. M. A.; Ribeiro, S. J. L.; Messaddeq, Y.; Dexpert-Ghys, J.; Verelst, M.; Dexpert, H. Synthesis and Luminescence Properties of Water Dispersible-Doped Boehmite Nanoparticles. *Nanotechnology* **2007**, *18* (45), 455605.
(34) Ram, S. Infrared Spectral Study of Molecular Vibrations in Amorphous, Nanocrystalline and AlO(OH)·αH2O Bulk Crystals. *Infrared Phys. Technol.* **2001**, *42* (6), 547−560.
(35) Frost, R. L.; Kloprogge, J. T.; Russell, S. C.; Szetu, J. Dehydroxylation of Aluminum (Oxo)Hydroxides Using Infrared Emission Spectroscopy. Part II: Boehmite. *Appl. Spectrosc.* **1999**, *53* (5), 572−582.
(36) Reichertz, P. P.; Yost, W. J. The Crystal Structure of Synthetic Boehmite. *J. Chem. Phys.* **1946**, *14* (8), 495−501.
(37) Saraswati, V.; Rao, G. V. N. X-ray Diffraction in γ-Alumina Whiskers. *J. Cryst. Growth* **1987**, *83* (4), 606−609.
(38) Luo, Z. Structure of Boehmite-Derived γ-Alumina and Its Transformation Mechanism Revealed by Electron Crystallography. *Acta Crystallogr., Sect. B* **2021**, *77* (5), 772−784.
(39) Prins, R. On the Structure of γ-Al2O3. *J. Catal.* **2020**, *392*, 336−346.
(40) Pakharukova, V. P.; Yatsenko, D. A.; Gerasimov, E. Yu.; Shalygin, A. S.; Martyanov, O. N.; Tsybulya, S. V. Coherent 3D Nanostructure of γ-Al2O3: Simulation of Whole X-ray Powder Diffraction Pattern. *J. Solid State Chem.* **2017**, *246*, 284−292.
(41) Paglia, G.; Buckley, C. E.; Rohl, A. L.; Hunter, B. A.; Hart, R. D.; Hanna, J. V.; Byrne, L. T. Tetragonal Structure Model for Boehmite-Derived γ-Alumina. *Phys. Rev. B* **2003**, *68* (14), 144110.
(42) Samain, L.; Jaworski, A.; Edén, M.; Ladd, D. M.; Seo, D.; Garcia-García, F. J.; Häussermann, U. Structural analysis of highly porous γ-Al_2O_3. *J. Solid State Chem.* **2014**, *217*, 1−8.
(43) Pigeon, T.; Chizallet, C.; Raybaud, P. Revisiting γ-Alumina Surface Models through the Topotactic Transformation of Boehmite Surfaces. *J. Catal.* **2022**, *405*, 140−151.
(44) Gan, T.; Chen, X.; Chu, X.; Jing, P.; Shi, S.; Zhang, Z.; Zhang, W.; Li, J.; Zhang, S.; Pavanello, M.; Wang, D.; Liu, G. "Atomic Topping" of MnOx on Al2O3 to Create Electron-Rich, Aperiodic, Lattice Oxygens That Resemble Noble Metals for Catalytic Oxidation. *J. Am. Chem. Soc.* **2024**, *146* (24), 16549−16557.
(45) Chalmin, E.; Farges, F.; Brown, G. E. A Pre-Edge Analysis of Mn K-Edge XANES Spectra to Help Determine the Speciation of Manganese in Minerals and Glasses. *Contrib. Mineral. Petrol.* **2009**, *157* (1), 111−126.
(46) Thommes, M.; Kaneko, K.; Neimark, A. V.; Olivier, J. P.; Rodriguez-Reinoso, F.; Rouquerol, J.; Sing, K. S. W. Physisorption of Gases, with Special Reference to the Evaluation of Surface Area and Pore Size Distribution (IUPAC Technical Report). *Pure Appl. Chem.* **2015**, *87* (9−10), 1051−1069.
(47) Dong, X.; Wang, D.; Lei, Y.; Yang, Y.; Liu, J. Construction of Rod-Shaped Manganese Trioxide/Phosphorus Doped Carbon Nitride Heterojunction for Z-Scheme Photodegrading Organic Pollutants. *J. Inorg. Organomet. Polym. Mater.* **2023**, *33* (9), 2890−2905.

https://doi.org/10.1021/acssusresmgt.5c00216
ACS Sustainable Resour. Manage. 2025, 2, 1906−1916

(48) Li, X.; Zhong, F.; Li, P.; Xiao, J.; Xi, J. Transition Metal Modified Al2O3 Mesoporous Nanospheres for Catalysis of Organic Reactions. *Appl. Surf. Sci.* **2024**, *653*, 159355.
(49) Shokri, A.; Shahhosseini, S.; Bazyari, A. Nanoporous Metatitanic Acid on γ-Al2O3 Aerogel for Higher CO2 Adsorption Capacity and Lower Energy Consumption. *Sci. Rep.* **2024**, *14* (1), 22905.
(50) Ferreira-Neto, E. P.; Worsley, M. A.; Rodrigues-Filho, U. P. Towards Thermally Stable Aerogel Photocatalysts: TiCl4-Based Sol-Gel Routes for the Design of Nanostructured Silica-Titania Aerogel with High Photocatalytic Activity and Outstanding Thermal Stability. *J. Environ. Chem. Eng.* **2019**, *7* (5), 103425.
(51) Zhou, X.; Yan, Y.; Zhao, Y.; Li, M.; Cui, W.; Shan, X.; Gao, Y.; Lyu, L.; Qian, Y. Organic-Inorganic Fiber Assembled ANFs/Al2O3 Hybrid Aerogel with Superelasticity and Multifunctionality. *Ceram. Int.* **2025**, *51* (17), 24274−24280.
(52) Alkhalaf, S.; Ranaweera, C. K.; Kahol, P. K.; Siam, K.; Adhikari, H.; Mishra, S. R.; Perez, F.; Gupta, B. K.; Ramasamy, K.; Gupta, R. K. Electrochemical Energy Storage Performance of Electrospun CoMn2O4 Nanofibers. *J. Alloys Compd.* **2017**, *692*, 59−66.
(53) Sharma, S.; Chand, P. Supercapacitor and Electrochemical Techniques: A Brief Review. *Results Chem.* **2023**, *5*, 100885.
(54) Beknalkar, S. A.; Teli, A. M.; Bhat, T. S.; Pawar, K. K.; Patil, S. S.; Harale, N. S.; Shin, J. C.; Patil, P. S. Mn3O4 Based Materials for Electrochemical Supercapacitors: Basic Principles, Charge Storage Mechanism, Progress, and Perspectives. *J. Mater. Sci. Technol.* **2022**, *130*, 227−248.
(55) Wang, B.; Li, Y.; Gu, Z.; Wang, H.; Liu, X.; Li, S.; Chen, X.; Liang, X.; Ogino, K.; Si, H. Biomass-Derived Hierarchically Porous Carbon-Supported MnOx Enable Fast Ion/Electron Transport at High Operating Voltages. *Fuel Process. Technol.* **2023**, *249*, 107857.
(56) Wu, X.; Zhan, T.; Sun, S.; Chen, W.; Yu, A.; Qiu, S.; Chen, L.; Qu, D.; Duan, J.; Li, X. In-Situ Electrochemical Preparation of MnOx/CC with Porous Structure and Mixed Valence for Supercapacitor. *Electrochim. Acta* **2025**, *516*, 145733.
(57) Samuel, E.; Joshi, B.; Kim, Y.; Aldalbahi, A.; Rahaman, M.; Yoon, S. S. ZnO/MnOx Nanoflowers for High-Performance Supercapacitor Electrodes. *ACS Sustain. Chem. Eng.* **2020**, *8* (9), 3697−3708.
(58) Luo, Y.; Li, J.; Chen, C.; Liu, W. ZnO-MnO2 Co-Modified Hierarchical Porous Carbon Nanofiber Film Electrodes for High-Energy Density Supercapacitors. *Sci. Rep.* **2025**, *15* (1), 6393.
(59) Fukuhara, M.; Yokotsuka, T.; Hashida, T.; Yamaguchi, K.; Fujima, N. Amorphous Alumina Supercapacitors with Voltage-Charging Performance. *Europhys. Lett.* **2023**, *141* (3), 36003.

https://doi.org/10.1021/acssusresmgt.5c00216
ACS Sustainable Resour. Manage. 2025, 2, 1906−1916